Case Studies in Engineering Failure Analysis 2 (2014) 100–106

Contents lists available at ScienceDirect

Case Studies in Engineering Failure Analysis

journal homepage: www.elsevier.com/locate/csefa

Case study

Fracture of a veneered-ZrO_2 dental prosthesis from an inner thermal crack

Ulrich Lohbauer [a,*], Renan Belli [a], Gerwin Arnetzl [b], Susanne S. Scherrer [c], George D. Quinn [d]

[a] Laboratory for Biomaterials Research, Dental Clinic 1 – Operative Dentistry and Periodontology, Friedrich-Alexander University of Erlangen-Nuremberg, Glueckstrasse 11, 91054 Erlangen, Germany
[b] Dental Clinic, University of Graz, Auenbruggerplatz 12, Graz, Austria
[c] Department of Prosthodontics-Biomaterials, School of Dental Medicine, University of Geneva, Switzerland
[d] ADAF Paffenbarger Research Center, NIST, Gaithersburg, MD, USA

ARTICLE INFO

Article history:
Received 16 May 2014
Received in revised form 6 June 2014
Accepted 12 June 2014
Available online 19 June 2014

Keywords:
Dental fractography
Dental ceramics
Dental prosthesis
Zirconia
Fracture
Thermal crack

ABSTRACT

Here we describe the fractographic analysis of a veneer-ZrO_2 single-unit dental prosthesis that fractured in a shell-like manner. Analysis of the retrieved fragment revealed that the crack originated in the bulk of the veneer from a thermal flaw located between two layers of the veneering material. Using the measured flaw plane we showed that the conditions of loading at fracture were complex and probably involved important tangential components.
© 2014 The Authors. Published by Elsevier Ltd. This is an open access article under the CC BY-NC-ND license (http://creativecommons.org/licenses/by-nc-nd/3.0/).

1. Introduction

Fracture in fixed dental prostheses (FDPs) can occur from multiple causes, and fractography has helped in the recent years to pinpoint several mechanisms and clarify the causes of failure in vivo [1–5]. Progress is made this way by educating dentists, technicians and manufacturers on the sensitive stages of manufacturing, processing, design, installation and maintenance. The ultimate goal is to minimize premature failures and extend the lifespan of prosthetic reconstructions.

Here we report on an unusual shell-like fracture pattern typical for FDPs made of porcelain veneered zirconium dioxide (ZrO_2). Reports on two similar cases are found in Ref. [6]. Shell-like fractures result in round fracture surfaces because the crack tends to deflect around the framework without reaching the interface [6,7]. Stress gradients in the veneer layer are suspected to contribute to this crack behavior [8,9]. In the present case a critical thermal flaw has been identified in the bulk of the veneer layer triggering the fracture. This flaw type is atypical and differs from the commonly observed crack initiating defects originating from contact damage or radial cracks from bending.

* Corresponding author. Tel.: +49 9131 854 3740; fax: +49 9131 853 4207.
E-mail addresses: ulrich.lohbauer@fau.de, lohbauer@dent.uni-erlangen.de (U. Lohbauer).

http://dx.doi.org/10.1016/j.csefa.2014.06.003
2213-2902/© 2014 The Authors. Published by Elsevier Ltd. This is an open access article under the CC BY-NC-ND license (http://creativecommons.org/licenses/by-nc-nd/3.0/).

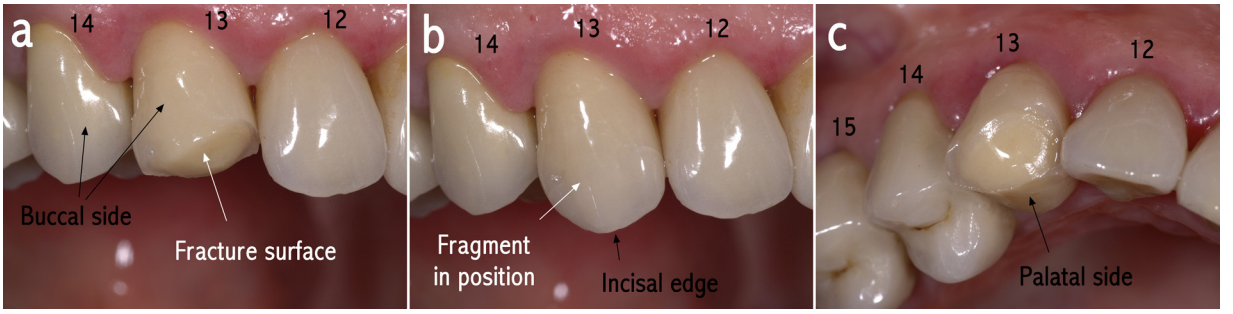

Fig. 1. (a) Buccal view of the clinical situation. The incisal third of the zirconia-veneered crown has fractured off. (b) Buccal view with the fragment in position. (c) Incisal view of the clinical situation. The fracture extended from palatal to buccal involving the whole circumference of the crown.

2. Background

The presented case deals with a fracture of a veneered-ZrO_2 single crown that took place during normal mastication (Fig. 1). The fracture event was reported to have occurred on May 24, 2011; the fragment was retrieved by the patient and brought to the dentist. The patient's record dated the installation to March 08, 2010, making it a 14 months and 16 days lifespan. The counterpart of the fragment remained attached to the tooth and had to be removed for purposes of restoration replacement and could not be further analyzed. The original fragment was received for analysis, along with the available material and processing information. According to the dentist, the affected tooth was an upper-right canine (FDI number system: #13) that had been restored with a veneered-ZrO_2 single crown. The framework material was a ZrO_2 (Yttria-stabilized Tetragonal Zirconia Polycrystals, 3Y-TZP) machined in a presintered state from a Zenotec Zr Disc (Wieland Dental, Pforzheim, Germany) having a coefficient of thermal expansion (CTE) of 10.5 ppm/°C. The overlaying veneering material was applied following the layering technique, in that successive layers of the veneering slurry are built-up anatomically over each other and sintered separately until the final anatomic form is reached. Usually between 2 and 5 layers can be needed for a single-unit dental FDP. The veneering material of the same manufacturer was an unreinforced porcelain (Zirox NR) of CTE = 9.3 ppm/°C. The antagonist was a natural tooth. This case was initially analyzed in June 2011 at the American Dental Association/NIST 2 day course on Dental Materials Fractography. It was more fully analyzed later in June 2012 and April 2014. A preliminary analysis of this case was published in [10].

3. Fractographic analysis

Optical and scanning electron microscopy (SEM-EDX) were used to analyze the piece. Optical images of the fragment are shown in different angles in Fig. 2. For better orientation, readers are referred to the diagram of an original structure (canine single-unit FDP) and the outline of the fracture edges and the internal fracture surface. On the fracture surface a distinct feature is observed some ~1 mm into the bulk (Fig. 3). This region in optical magnification reveals a circular convex plane that differs from the other planes on the fracture surface (note the variations in light reflection), and is delimited at the upper part by an angular border. An elongated flaw is located at the midline of this border and appears flat, smooth an shiny. By tilting the fragment the "outer veneer", the "inner veneer" and the flaw seem to have distinct surface planes. The "outer veneer" formed a sharp angle with the external surface, whereas the plane of the flaw deviated from the "outer veneer" plane toward the y-axis (see Fig. 6 for coordinates). The fracture surface was scanned using a non-contact white-light optical profilometer (CyberSCAN CT 100, Cyber Technologies, Ingolstadt, Germany) to measure these angles (Fig. 5). The angle between the "outer veneer" and the external palatal surface was 55°, and the angle between the "outer veneer" and the flaw plane was 131°. This results in an angle of 76° between the flaw plane and the contact surface. The angle between the flaw plane and plane of crack propagation ("inner veneer" in Fig. 3) was 156°. Using the scan data the depth of the flaw into the bulk was determined to be 820 μm.

From the elongated flaw, concentric "ringing" lines developed inward to an extension of 1–1.5 mm (Fig. 3). These are *Wallner lines*, which form as ripples from the crack propagation event and indicate the primary direction of crack propagation. Figure 4 consists of a composite of several images from the gold-coated fragment to form a single focused image. The better contrast highlights the outer edges of the fragment and reveals a ~0.8 mm-thick flat margin around most of the fragment in a ~90° angle with the external surface. The inner edge of this margin circumscribes the concave region on the fracture surface. Further, Fig. 4 shows a composition of SEM images showing the palatal and the fracture surfaces of the fragment. On the palatal surface a track of occlusal wear is clearly distinguishable from the unworn surface, indicating the activity of antagonistic contact on the region of fracture. Moving down in the image, a hackle line connects the fracture originating flaw to the outer edge of the fracture. This is a resulting intersection line that formed in a second stage of fracture, when the crack path went around the origin site to complete the fracture (Fig. 6). The backscattered mode in the SEM revealed no difference between the "outer veneer" and the "inner veneer". A close-up of the fracture initiating flaw is seen in Fig. 5b, and shows no particular material irregularity, but a flat surface measuring 48 μm in the short axis and 180 μm in the

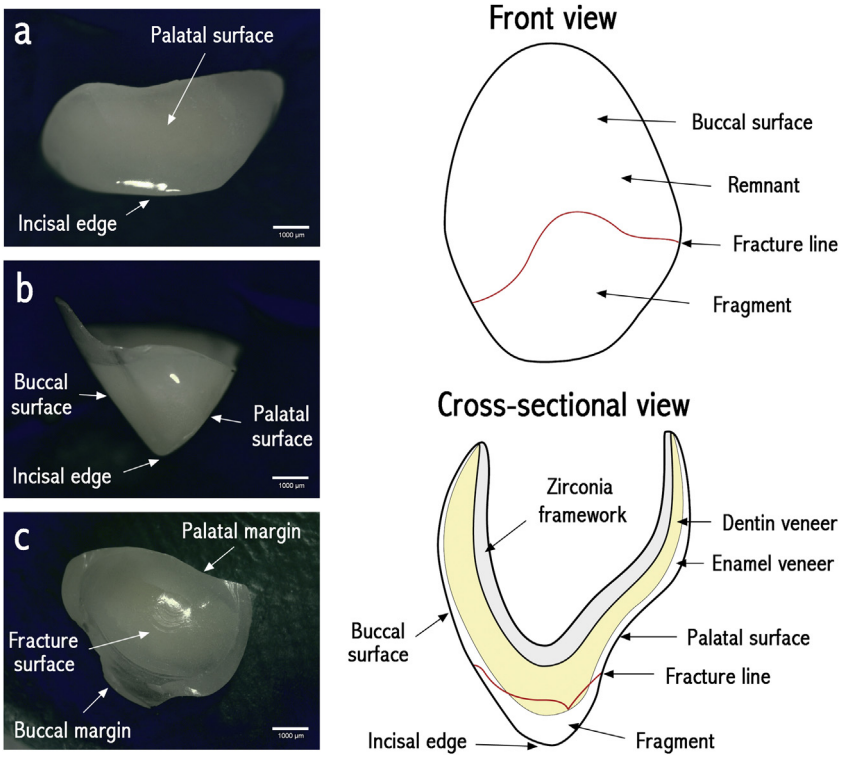

Fig. 2. Images (a–c) show optical microscopy images of the recovered fragment from different views. The reader is referred to the diagram on the right-hand side and to the legends for better understanding.

long axis, with sharp extremities. An EDX analysis was conducted on different regions of the piece, as seen in Fig. 4. Common elements for all areas were those typical for porcelain materials, such as Al, K, Si, and Ca. On the fracture surface in the "inner veneer" high amounts of Cu and Fe were found, elements that were scarce on the external surface of the piece, where additional traces of Ti were found.

4. Causes of failure and discussion

Embedded in the bulk of the porcelain we found a well-defined flat and smooth flaw that related well to markings of the initial stages of crack growth. The original fracture-triggering flaw was not a contact crack, which are typically found on

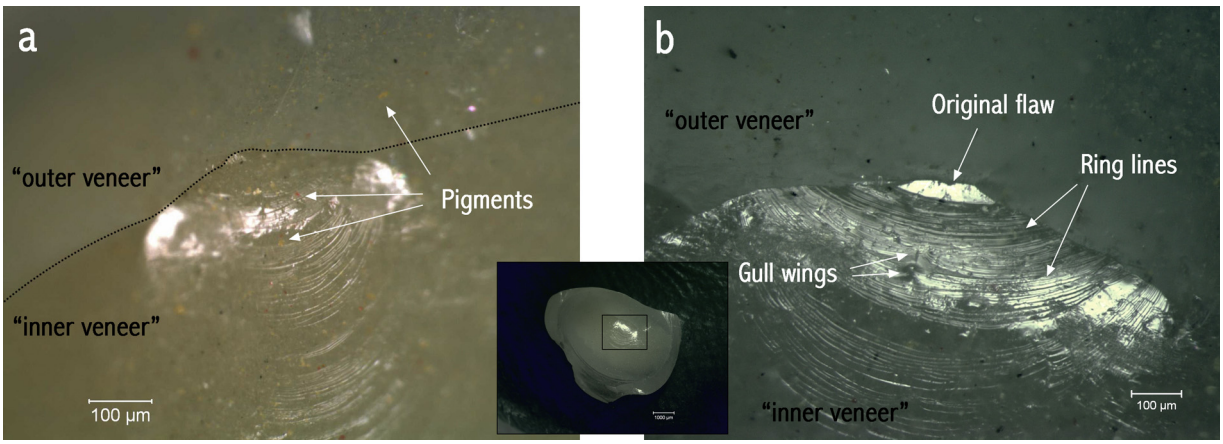

Fig. 3. Optical microscopy images of the fracture surface showing the fracture origin site in magnification. Note the convex plane at the center. In (a) two regions are delimited above and below the upper border of the convex plane and designated "outer veneer" and "inner veneer". Shade and translucency can be distinguished between these two regions. Yellow and red crystal pigments can be seen through the porcelain. In (b) the light source is made perpendicular to the plane of the origin flaw, which shows a flat and reflective surface. From the flaw downward, ring "Wallner" lines formed concentrically at the first stages of crack growth. (For interpretation of the references to color in this figure legend, the reader is referred to the web version of this article.)

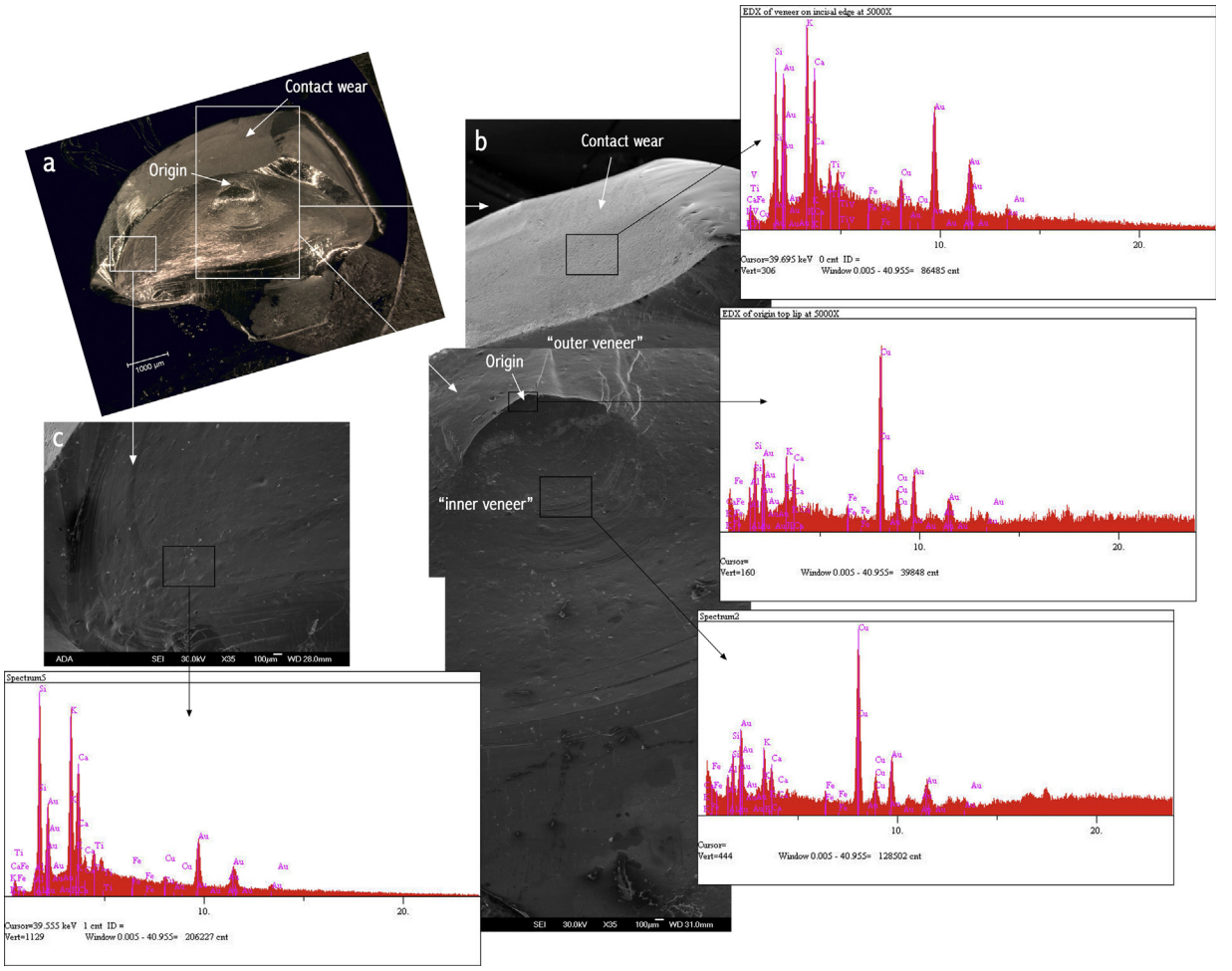

Fig. 4. SEM images of the palatal and fracture surfaces of the fragment. EDX maps from different regions of the fragment are indicated accordingly. Note the presence of Cu on the ''inner veneer'' and its absence on the ''outer veneer''.

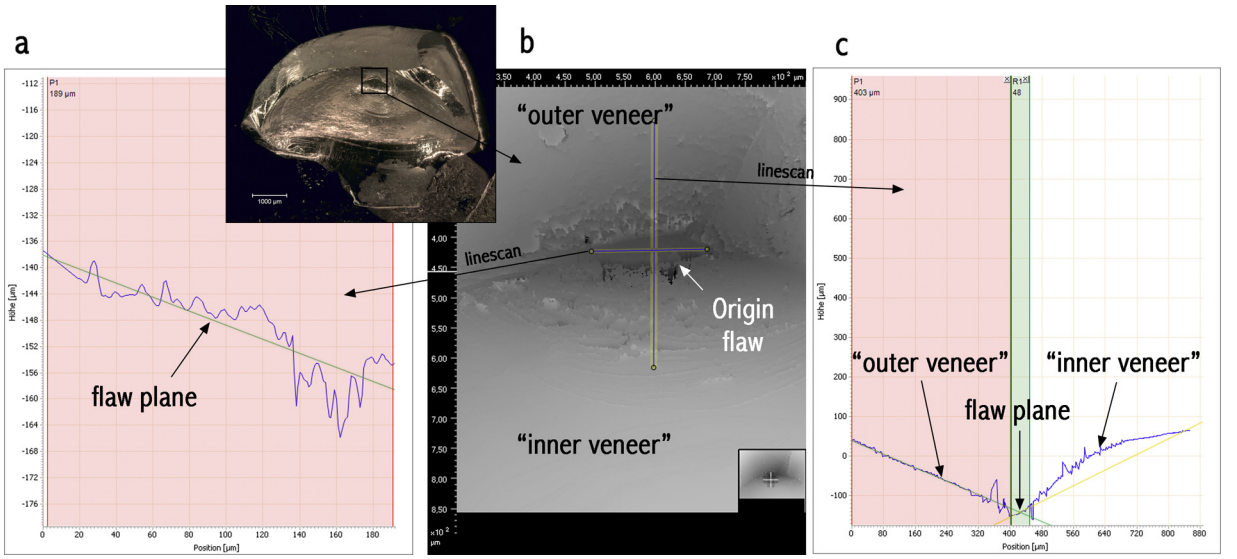

Fig. 5. Optical profilometry of the fracture origin site (b). Linescans through the origin flaw show the inclination planes in its long axis (a) and short axis (c). In (c) the angle between the ''outer veneer'' plane and the flaw plane is measured. Note the steep plane of the ''inner veneer'' in comparison to the flaw plane.

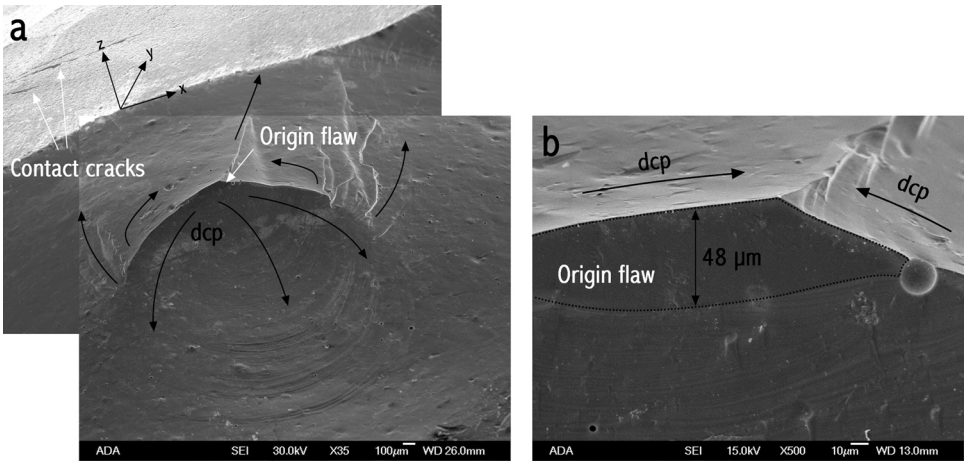

Fig. 6. SEM magnification images of the origin site (a) and the flaw triggering fracture (b). In (a) the direction of crack propagation (dcp) shows how the crack first propagated inward and only later outward to complete the fracture. In (b) the flaw morphology is to be observed. Note in (a) the spacial coordinates that help to put fracture planes in perspective. The "*y*" plane is the plane of the palatal surface, whereas the "*z*" plane characterizes the depth into the bulk.

FDPs? contact surfaces and triggering failure, but rather a thermally created flaw. Thermal cracks are usually very smooth and reflective. The fracture originating from this flaw first developed inward (into the bulk), and only outward (toward the palatal surface) in the last moments of fracture, when the crack completed a full-circle around itself. The location depth and the surface plane of the flaw in relation to the external palatal surface suggests that it may have been located between two layers of veneering material that were built-up and fired separately. Thermal stresses probably developed at the interface during this process. The fact that the EDX readings on the external surface and on the "inner veneer" resulted in slightly different compositions supports this hypothesis. The "inner veneer" contained high amounts of copper, which in the oxide form Cu_2O is a red pigment used in dental porcelains along with Fe_2O_3, for recreating the saturated yellow-brownish shade of the dentin tissue. In the optical image in Fig. 3a, a multitude of red and yellow spots are seen dispersed in the porcelain, probably the crystals of Cu_2O (red) and Fe_2O_3 (yellow). The outer surface gave less readings of these elements, characterizing a more translucent material, usually used to mimic the milky opalescent dental enamel (TiO_2 confers a whitish appearance). It is very unusual to find a fracture origin located at the interface between veneer layers. If our hypothesis is true, the flaw triggering the fracture originated during the laboratorial manufacturing of the piece as a result of the layering procedure.

Interestingly the fracture did not initiate from contact damage, which creates high tensile stress zones around the indenter, but rather deep in the bulk of the veneer where tensile stresses are much lower. From the optical images one can observe that the plane of the internal flaw was neither orthogonally (*z*-axis) nor parallel oriented with respect to the external surface (*xy* plane) (see Fig. 6 for coordinates). Cracks in such orientation are more susceptible to the shear components of the stress field in a normally oriented load scenario. Although longer and sharper in the long axis (*x*-axis), the flaw grew in a direction similar to the plane of its short axis for several hundred micrometers to form a distinguished circular convex plane on the fracture surface. The location depth of the flaw (820 μm) is also an important piece of information.

From the fractographic evidence, one scenario is that thermal stresses created an initial flaw at the veneer layer interfaces during fabrication. These stresses are often transient and localized, so the crack did not propagate all the way through the crown. The crown was installed, and only later fractured in vivo. Another possibility is that the initial flaw was not present during installation, but popped in later in vivo due to combined residual stresses in the veneer and occlusal surface contact stresses. Analysis of transient thermal stresses, or residual stresses in the veneer coupled with localized contact stresses is a formidable problem.

Rough estimates of the stresses that may have been acting on the origin flaw can be made as follows. We start with the stress field from contact of the crown with the antagonist tooth under the contact using the classic Hertzian contact mechanics solutions to determine the magnitude of stresses at the depth in which the fracture originated. Usually cracks form at the contact surface in Hertzian contact stress problems. One possibility is that part of the contact crack did extend to the palatal surface in the missing fragment, but the plane of fracture of the initial crack suggests this was not likely. The other scenario is that contact stresses "reached down" into the bulk of the veneer and triggered fracture initiation underneath the surface. The radius of the circular contact *a* between a round indenter (in this case the cusp of the antagonist tooth) and a flat surface (the palatal surface of the FDP) take the form:

$$a = \left[\frac{3}{4} P R_C \left(\frac{1-\nu_A^2}{E_A} + \frac{1-\nu_S^2}{E_S}\right)\right]^{1/3} \tag{1}$$

where the subscripts *A* and *S* refer to "antagonist" and "substrate", respectively, *P* is the load applied, the relative radius $R_C = 1/R_A + 1/R_S$ (for a flat substrate $R_S \to \infty$), ν is the Poisson's ratio and *E* the Young's modulus. The radius of the antagonist was taken to be 1.5 mm, *E* and ν of human enamel 90 GPa and 0.27, whereas 65 GPa and 0.21 are typical *E* and ν values for

dental porcelains. The principal stresses σ_1, σ_2 and σ_3 as a function of the depth (along the z-axis) under the indenter are calculated using:

$$\sigma_1 = \sigma_2 = \sigma_x = \sigma_y = -p_0\left[(1+\upsilon)\left(1-\left|\frac{z}{a}\right|\arctan\left|\frac{a}{z}\right|\right) - \frac{1}{2((z^2/a^2)+1)}\right] \tag{2}$$

and

$$\sigma_3 = \sigma_z = -p_0\left(\frac{z^2}{a^2}+1\right)^{-1} \tag{3}$$

where p_0 is the peak contact pressure at the center given by:

$$p_0 = \frac{3P}{2\pi a^2} \tag{4}$$

The maximum shear stresses are then:

$$|\tau_{xz}| = |\tau_{yz}| = \tau_{\max} = \left|\frac{\sigma_1 - \sigma_3}{2}\right| = \left|\frac{\sigma_2 - \sigma_3}{2}\right|. \tag{5}$$

For a 100 N normal load, immediately under the indenter the principal stresses are compressive up to −1670 MPa. At around 160 μm from the surface σ_1 and σ_2 become tensile, and reach their maximum value of 29 MPa at around z = 250 μm. At the flaw depth (z = 820 μm) σ_1 and σ_2 decrease to 6.3 MPa, and $\tau_{\max}$ = 37.5 MPa. The maximum value of the shear stresses τ_{12} and τ_{23} are located at circa 0.5a and reach 794 MPa.

It is however difficult to determine at which load the fracture occurred, considering the wide amplitude of chewing loads taking place in the mouth (up to several hundreds of Newtons). The upper canine is a special case per se once its palatal surface serves as the sole lateral guidance for disocclusion in patients with no group function. This concentrates all the load in a single point and stresses go up accordingly. In Fig. 7 a plot of the stress components $\sigma_{1,2}$ and $\tau_{\max}$ under the indenter (along the z axis) under normal loading is given for loads ranging from 100 to 400 N. The average shear strength for dental porcelains serves as reference. Using the criterion $\tau_{\max} \geq \sigma_{\text{shear}}$ (the ultimate shear strength for dental porcelains (∼130 MPa [11])), loads >400 N would be necessary to cause fracture due to a single overloading event. The presence of the flaw is sure to have further degraded the material's strength, reducing the load needed to cause fracture. Also the effect of probable residual stresses in the veneer due to the high CTE mismatch should not be ruled out.

Our scans of the fracture surface revealed that the first stages of crack growth further deviated the crack plane from the axis of normal loading, resulting in a kink angle of ∼24°. This is a strong indication of a mixed mode condition, and suggests that the loading at fracture was not normally oriented. On the palatal surface of the fragment evidences of sliding wear are found with accompanying partial cone cracks (see Fig. 6, upper left corner), indicating that a tangential loading component was also active during crack initiation. When a tangential force component exists during loading (as in the case of tooth-tooth sliding contact), the maximum shear stress increases due to friction and take the form of the solutions derived by

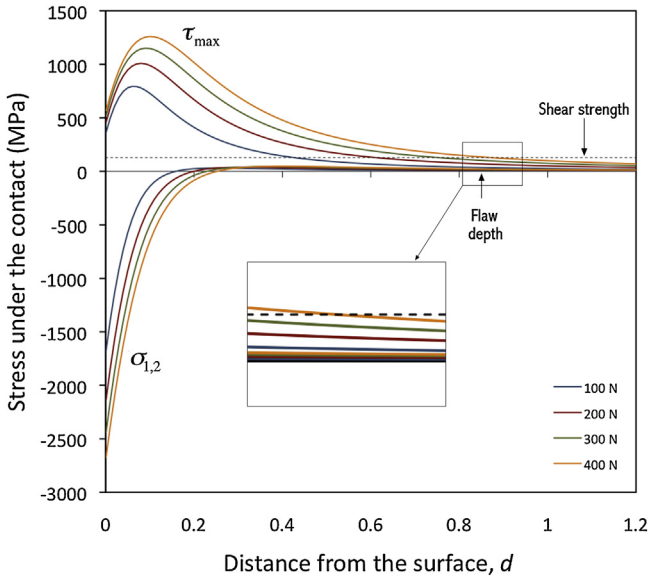

Fig. 7. Plot of the unnormalized values (in respect to p_0) of the Hertzian principal stresses $\sigma_{1,2}$ and the shear stress $\tau_{\max}$ along the z axis under the contact for different loads. Note at the flaw depth how the principal stresses are tensile approaching zero. The dashed line is the ultimate shear strength of the material.

Hamilton [12]. The crack tip under mixed mode loading feels the tensile and the shear components of the stress, and deflects to a more favorable orientation from its original plane. According to some available fracture criteria for mixed mode loading, the crack propagates onto the direction perpendicular to the maximum tensile normal stress (maximum normal stress criterion [13]) or to the plane of the maximum energy release rate (maximum energy release rate criterion [14]), where the mode-II stress intensity factor disappears. From our measurements this plane formed a 52° angle to the palatal contact surface (Fig. 5).

5. Conclusions and recommendations

Our fractographic analysis showed that fracture of dental prostheses may initiate from internal thermal flaws, and not exclusively from contact cracks, radial cracks or marginal defects. The fracture origin in the presented case was a thermal flaw that resulted from the layering technique. Fracture was prompted by sliding contact loading and expedited by an internal flaw embedded in a veneering material under considerable thermal residual stresses. Other manufacturing techniques that avoid incremental sintering of the veneer might come as a more reliable option. Assessing the orientation of the flaw to the external surface allowed us to state on the complex nature of the load scenario that prompted the fracture.

References

[1] Kelly R, Giordano R, Pober R, Cima MJ. Fracture surface analysis of dental ceramics: clinically failed restorations. Int J Prosthodont 1990;3:430–40.
[2] Lohbauer U, Amberger G, Quinn GD, Scherrer SS. Fractographic analysis of a dental zirconia framework: a case study on design issues. J Mech Behav Biomed Mater 2010;3:623–9.
[3] Scherrer SS, Quinn GD, Quinn JB. Fractographic failure analysis of a Procera AllCeram crown using stereo and scanning electron microscopy. Dent Mater 2008;24:1107–13.
[4] Scherrer SS, Quinn JB, Quinn GD, Kelly JR. Failure analysis of ceramic clinical cases using qualitative fractography. Int J Prosthodont 2006;19:185–92.
[5] Scherrer SS, Quinn JB, Quinn GD, Wiskott HW. Fractographic ceramic failure analysis using the replica technique. Dent Mater 2007;23:1397–404.
[6] Belli R, Scherrer SS, Reich S, Petschelt A, Lohbauer L. In vivo Shell-like fractures of veneered-ZrO_2 fixed dental prostheses. Case Stud Eng Fail Anal 2014;2:91–9. http://dx.doi.org/10.1016/j.csefa.2014.06.001.
[7] Belli R, Petschelt A, Lohbauer U. Thermal-induced residual stresses affect the fractographic patterns of zirconia-veneer dental prostheses. J Mech Behav Biomed Mater 2013;21:167–77.
[8] Belli R, Monteiro Jr , Baratieri LN, Katte H, Petschelt A, Lohbauer U. A photoelastic assessment of residual stresses in zirconia-veneer crowns. J Dent Res 2012;91:316–20.
[9] Swain MV. Unstable cracking (chipping) of veneering porcelain on all-ceramic dental crowns and fixed partial dentures. Acta Biomater 2009;5:1668–77.
[10] Quinn GD. Fractographic analysis of broken ceramic dental restorations. Ceram Eng Sci Proc 2014 [in press].
[11] Johnston WM, O'Brian WJ. The shear strength of dental porcelain. J Dent Res 1990;59:1409–11.
[12] Hamilton GM. Explicit equations for the stresses beneath a sliding spherical contact. Proc Inst Mech Eng C: J Mech Eng Sci 1983;197C:53–9.
[13] Erdogan F, Sih GC. On the crack extension in plates under plane loading and transverse shear. J Basic Eng 1963;85:519–27.
[14] Hussain MA, Pu SL, Underwood J. Fracture Analysis. ASTM STP 560. Philadelphia, PA: ASTM; 1974. p. 2–28.